Applied Physics B (2024) 130:170
https://doi.org/10.1007/s00340-024-08306-w

RESEARCH

Analysis of Cs solution by nano-silica particles-enhanced laser-induced breakdown spectroscopy

Shujia Wu[1,2] · Chen Yang[1] · Juhao Yue[1] · Zexuan Wang[1] · Jiaxing Yang[1] · Shaohua Sun[2] · Bitao Hu[2] · Zuoye Liu[2]

Received: 22 May 2024 / Accepted: 18 August 2024

Abstract
Nanoparticle-enhanced laser-induced breakdown spectroscopy (NELIBS) represents a promising tool for detecting trace elements. This work improves NELIBS by substituting metal nanoparticles with nano-silica particles to achieve rapid detection of Cs elements at low concentrations. This substitution effectively prevents cluster formation and simplifies the experiment preparation process. The research optimizes factors such as target movement speed, nanoparticle concentration, and nanoparticle size to identify the optimal experimental parameters. Comparative analysis of the 3D morphology of laser ablation areas with and without nanoparticles reveals that evenly distributed nano-silica particles on the target surface provide the most effective colloidal particle lens array (CPLA) effect, and increasing the roughness of the target surface thereby enhancing the quality of laser ablation. With a laser frequency of 10 Hz, optimal characteristic spectral signals are achieved when the target movement speed exceeds 2 mm/s. Under conditions of a concentration of 0.1 mg/mL and an average particle size of 50 nm, the greatest enhancement effect on Cs element LIBS characteristic spectral signals is observed. Consequently, the limit of detection (LOD) and the limit of quantitation (LOQ) of elemental Cs by LIBS technology are reduced to 0.45 mg/L and 1.51 mg/L, respectively, facilitating real-time detection of Cs element at low concentrations. In addition, the nano-silica particles have also had a certain enhancement effect on the spectral signal of elemental properties in the target, proving that enhancing the LIBS characteristic spectral signal using nano-silica particles is a feasible method.

1 Introduction

Nuclear energy serves as one of the main clean energy sources, playing a significant role in energy conservation and emission reduction, particularly in fields like electricity generation and heating. Nevertheless, the leakage of radioactive nuclides from nuclear power plants into the environment poses irreversible harm to organisms and ecosystems, with cancer being the predominant health risk [1, 2]. ^{137}Cs, characterized by its relatively high radioactivity and a half-life of 30 years, persists in the environment and tends to accumulate in living organisms [3]. Prolonged exposure to ^{137}Cs-containing radioactive materials substantially elevates the risk of various cancers, including liver, thyroid, and kidney cancer, as well as leading to severe genetic disorders. Therefore, the development of rapid and effective detection methods for radioactive nuclides such as ^{137}Cs is imperative for nuclear safety. Currently, gamma rays emitted from the decay of ^{137}Cs are detected using high-purity germanium detectors to quantify the concentration of radioactive substances. Despite this method has low collection efficiency and requires a long time for data accumulation. Laser-induced breakdown spectroscopy (LIBS) technology, emerging as a promising detection method, enables qualitative or quantitative analysis of elements in samples by analyzing the emission spectrum of plasma generated on the sample surface through laser ablation [4, 5]. Due to its capability to simultaneously detect multiple elements, LIBS has found widespread applications in areas such as agricultural product pollution [6], atmospheric pollution [7], soil pollution [8], ore discrimination [9], and other environmental analyses fields [10].

In LIBS characteristic spectra, the physical and chemical properties of isotopes belonging to the same element

✉ Zuoye Liu
zyl@lzu.edu.cn

[1] Frontiers Science Center for Rare Isotopes, Lanzhou University, Lanzhou 730000, China

[2] School of Nuclear Science and Technology, Lanzhou University, Lanzhou 730000, China

Published online: 02 September 2024

demonstrate a high degree of uniformity. However, variations in mass numbers inevitably induce specific deviations in the characteristic spectral signals of LIBS. For instance, deuterium demonstrates a characteristic wavelength blue shift compared to hydrogen [11, 12], while ^{13}C exhibits a red shift of approximately 0.5 nm relative to ^{12}C [13]. Consequently, researchers extensively employ isotopes of radioactive nuclides to assess LIBS detection performance for elements such as U, Gd, etc. [14, 15]. Metzinger A [16] employed liquid-solid conversion to detect Cs in urine, achieving detection limits of 6 ng in urine samples and 27 ng in serum samples with a sample volume of 1 μL. They also noted that Cs isotope detection could be accomplished provided that the spectrometer's resolution is sufficiently high. Similarly, Ramli M [17] utilized LIBS technology to measure Cs content in water and soil under low-pressure conditions. They concluded that LIBS could potentially replace germanium detector gamma-ray spectroscopy for detecting Cs content in water and soil near nuclear power plants. Nevertheless, the sensitivity of LIBS detection is affected by factors like sample uniformity, laser energy fluctuations, and spectrometer stability, etc. In laboratory settings, it is often combined with signal enhancement methods such as dual-pulse [18, 19], microwave-assistance [20], cavity-confinement [21], and nanoparticle enhancement [22] to achieve improved detection sensitivity. However, dual-pulse and microwave-assistance enhancement methods necessitate additional equipment (laser or microwave generators) to reheat the plasma; cavity-confinement enhancement methods are suitable for solid samples, compressing the plasma by reflecting shock waves to obtain more stable LIBS spectral signals. Nanoparticle-enhanced laser-induced breakdown spectroscopy (NELIBS) only requires coating the target surface with a layer of nanoparticles to achieve signal enhancement. Nano-gold particles have been utilized to achieve stable enhancement effects on LIBS characteristic spectral signals [23]. Nonetheless, during the drying process on the target surface, nanoparticles tend to form clusters, affecting laser focusing and resulting in varying enhancement results of LIBS signals at different areas on the surface, thereby reducing detection repeatability. It is imperative to regulate the interaction between nano-gold particles and inhibit cluster formation by altering solvents, adding dispersants, and employing other methods. In comparison to nano-gold, the preparation process of nano-silica particles is more mature, with better sphericity. These particles exhibit excellent dispersion in solution and typically do not necessitate the addition of external reagents to prevent clustering, offering a new option for NELIBS. When nano-silica particles are evenly spread on the target surface, the phenomenon of colloidal particle lens array (CPLA) occurs, while increasing the roughness of the target surface, which can enhance the laser ablation effect on the target surface [24, 25]. Moreover, Cabalín [26] has demonstrated that the LIBS emission signal for a single ablation pulse is dependent on the surface roughness. Lopez-Quintas et al. [27] have directly pointed out that the characteristic parameters of LIBS spectra, such as spectral line intensity and integral area, monotonically increase with the rise in sample surface roughness. Therefore, the deposition of nanoparticles on the surface of a smooth target has been shown to increase the target's surface roughness, thereby enhancing the LIBS spectral signal.Drawing on this premise, the current study endeavors to enhance the detection sensitivity of LIBS technology for Cs element. It investigates the effects of nano-silica particles with varying concentrations and particle sizes on LIBS characteristic spectral signals. Through the identification of optimal experimental conditions, the study aims to enhance the emission spectra of Cs element, thereby enhancing the quantitative detection sensitivity of LIBS technology for Cs element.

2 Experimental setup and samples

Figure 1 illustrates the schematic diagram of the LIBS experimental setup. comprising a Nd: YAG laser (Powerlite 9010, Continuum, USA), a grating spectrometer (Mechelle 5000, Oxford Instruments, UK), equipped with an enhanced camera (Andori Star DH-334T-18U-03, ANDOR, UK), a digital pulse delay controller (DG645, Stanford Research System, USA), a sample stage controller (TMC-USB, Zolix Instruments Co., Ltd., China), and a computer. During measurements, the laser operates at a wavelength of 532 nm, a frequency of 10 Hz, and an energy of 40 mJ adjusted using a half-wave plate and polarizer. To mitigate emission spectral interference caused by laser breakdown in the air, the laser is focused using a plano-convex lens with a 100 mm focal length, positioning the laser focal point 1 mm inside the target material from its surface. The digital pulse delay controller provides precise external trigger signals for both the pulsed laser and spectrometer. The spectrometer gain is set to 500, with a collection delay of 500 ns and a gate width of 5 μs, to collect plasma emission spectrum data in the wavelength range of 230 nm to 855 nm. To prevent the effect of uneven diffusion of Cs solution on the target surface during the drying process, for each sample, seven LIBS spectra are collected, with each spectrum accumulated from 8 laser pulses at random positions on the target surface.

The target utilized is a high-purity Al sheet measuring 50 mm * 30 mm * 1 mm. Prior to each measurement, the target surface undergoes rinsing with alcohol followed by a 15-minute ultrasonic cleaning process and then natural air-drying. To prepare the intermediate solution with a Cs

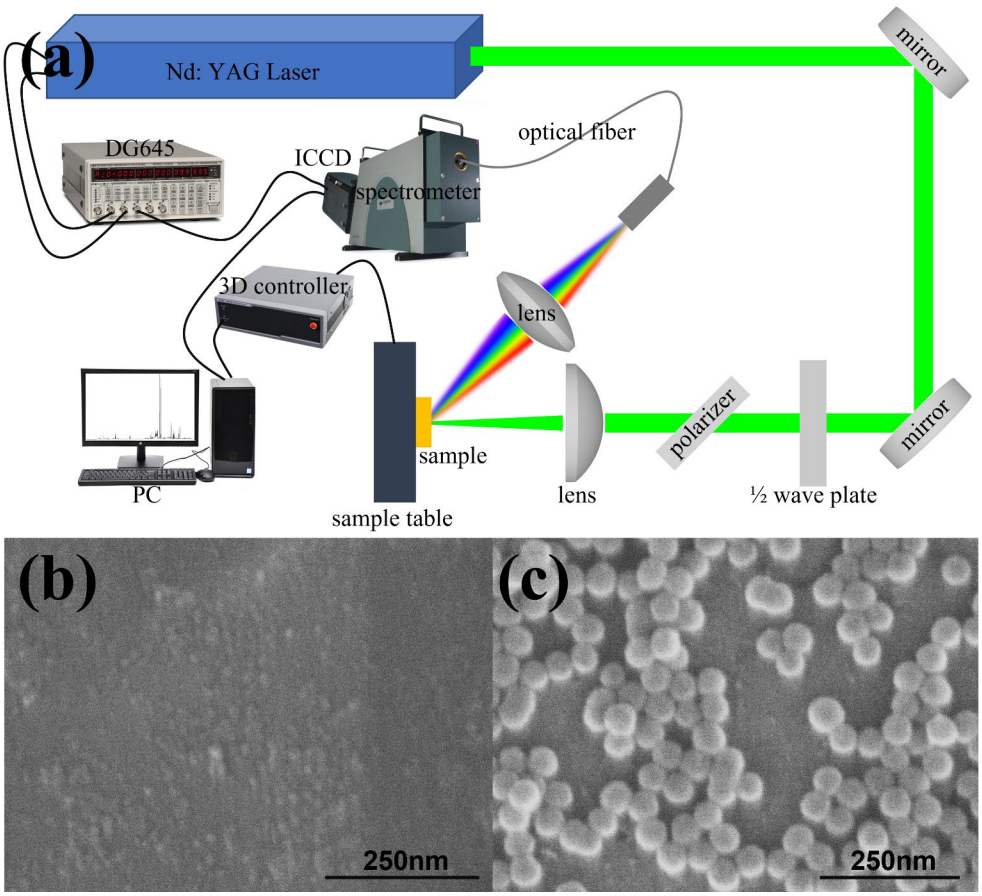

Fig. 1 Instruments and targets. (**a**) schematic diagram of LIBS setup; (**b**) no nano-silica particles on the target surface; (**c**) with nano-silica particles on the target surface

concentration of 1000 mg/L, 0.0289 g of cesium acetate is dissolved in 20 mL of alcohol. Subsequently, 4 mL of the intermediate solution is mixed with 6 mL of alcohol to yield the final solution with a Cs concentration of 400 mg/L. During sample preparation, varying volume ratios of the final Cs solution, nano-silica particles solution, and alcohol solution are controlled to produce mixed solutions with different concentrations of Cs and nano-silica particles. A 200 µL aliquot of the mixed solution is deposited onto the target surface and allowed to air-dry naturally. Following drying, the surface morphology of the target is examined using a scanning electron microscope (SEM), depicted in Fig. 1(b) and Fig. 1(c). Alcohol, compared to traditional solvents, significantly reduces the natural drying time, thereby enhancing the sample detection rate.

3 Results and discussion

For LIBS measurements, optimizing various factors is crucial, as depicted in Fig. 2, which outlines the specific optimization details of this study. Figure 2(a) illustrates LIBS spectra under four different conditions. The LIBS spectra are normalized for clear visualization of spectral comparisons. It is evident that rich Si element characteristic spectral lines are excited in the cases of "Nano-silica" and "NELIBS". In the cases of "LIBS" and "NELIBS", a distinct Cs I 852.11 nm characteristic peak is observed, indicating that impurity components in the target do not include Cs element and thus will not introduce interference with the measurement. In addition, the characteristic peak of Cs I 852.11 nm has been selected as the analytical spectral line, and the target moving velocity V_Y has been optimized to reduce the influence of laser ablation area overlap on the characteristic spectrum of Cs element LIBS. As depicted in Fig. 2(b), when $V_Y < 2$ mm/s, the larger coincidence of the laser focal point area leads to repeated laser pulse impacts on the same area of the solution on the target surface, resulting in a low intensity of the Cs element characteristic spectral lines being excited. Conversely, when V_Y is too large, the number of data points collected on the target surface in a single LIBS spectrum decreases. Therefore, the wavelength range from 832.04 nm to 838.03 nm is selected as the background spectrum. The signal-to-noise ratio (SNR) is obtained by the ratio of the characteristic spectral line intensity to the standard deviation of the background spectrum. Through the combination of characteristic spectral line intensity and

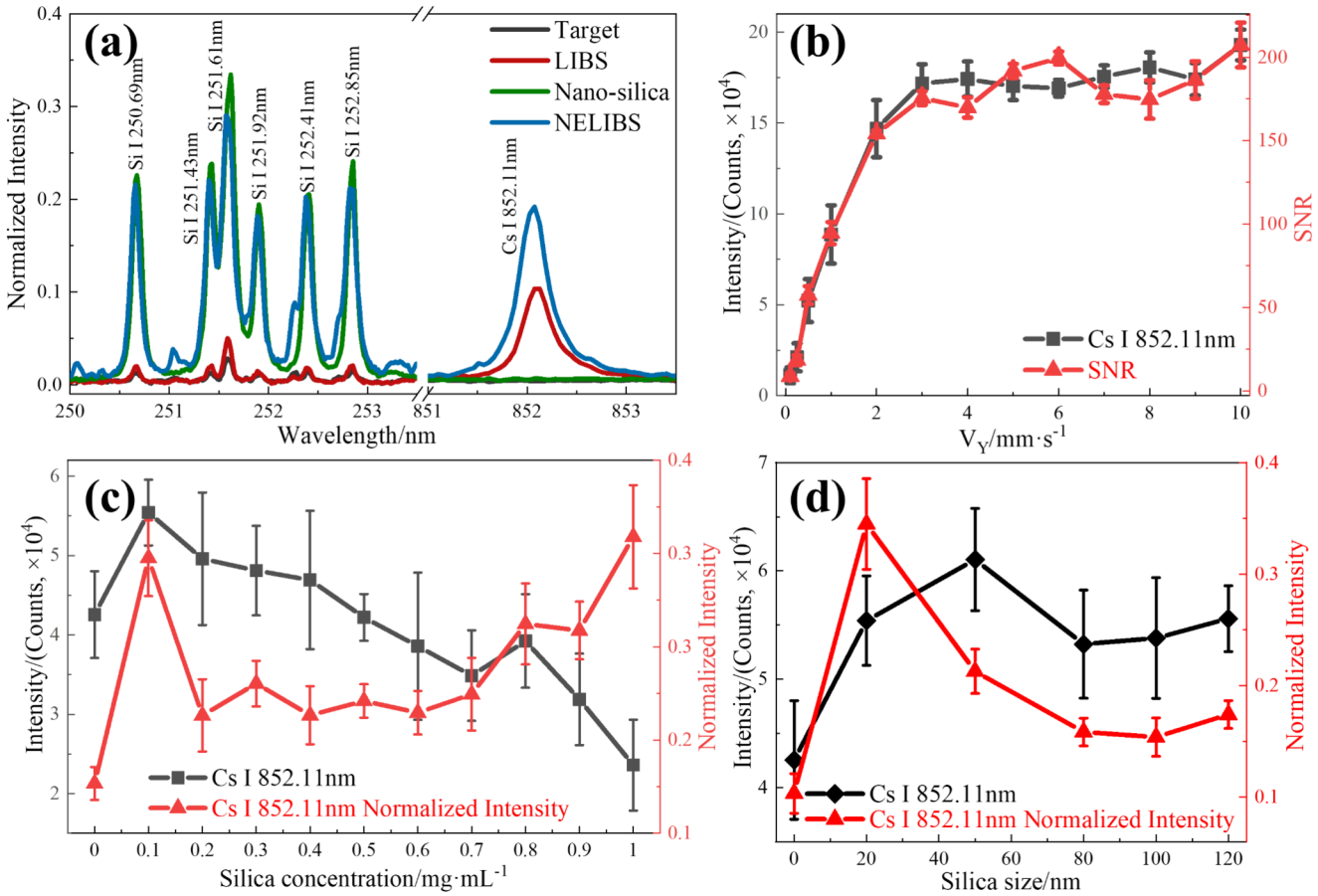

Fig. 2 (**a**) LIBS spectra under different conditions. "Target": Only 200 μL alcohol solution is added to the surface of the target for LIBS spectrum acquisition; "LIBS": Only 200 μL Cs solution (100 ppm) is added to the surface of the target for LIBS spectrum acquisition; "Nano-silica": Only 200 μL nano-silica particles solution (20 nm, 0.5 mg/L) is added to the surface of the target for LIBS spectrum acquisition; "NELIBS": A mixture of 200 μL Cs and nano-silica particles (Cs concentration 100 ppm, nano-silica particles size and concentration 20 nm, 0.5 mg/L, respectively) is added to the surface of the target for LIBS spectrum acquisition.; (**b**) Influence of target motion speed V_Y on analytical spectral lines; (**c**) Influence of nano-silica particles concentration on analytical spectral lines; (**d**) Influence of nano-silica particles size on analytical spectral lines

SNR, $V_Y = 6$ mm/s has been determined to be the optimal target movement speed for this experiment.

Previous research suggests that the concentration of nanoparticles directly influences the enhancement effect of NELIBS characteristic spectra [28]. Therefore, optimizing the nanoparticle concentration is essential. To achieve this, 100 μL of cesium acetate solution (400 ppm) is individually added to centrifuge tubes, and the nanoparticle concentration is adjusted by varying the volume ratio of anhydrous ethanol to nano-silica particles solution. The total volume of the solution within the centrifuge tubes is precisely set at 400 μL, after complete mixing, 200 μL of each solution is dispensed onto the target surface and left to air dry.

Figure 2(c) depicts the impact of nano-silica particles concentration on the intensity of analytical spectral lines with a fixed Cs element concentration. When the concentration of nano-silica particles is below 0.4 mg/L, it moderately enhances the intensity of the analysis spectral line. Additionally, an optimal enhancement effect on Cs element is observed at a nano-silica particles concentration of 0.1 mg/ mL. However, as the concentration of nano-silica particles increases, the intensity of the analysis spectral line exhibits a declining trend. This decrease can be attributed to the increase in nano-silica particles concentration, there is a rapid increase in the probability of forming a thick nano-layer on the target surface, which obstructs the laser from reaching the target surface, thus reducing the efficiency of laser ablation [29]. After the maximum intensity normalization of the entire LIBS spectrum, it has been found that the intensity of the analysis spectral line initially decreases and then increases. This phenomenon arises from the addition of low-concentration nano-silica particles, which promotes a more even spreading effect on the target surface, enhancing the focusing efficiency of the incident laser and contributing to its uniformity. However, with increasing nano-particle concentration, irregular stacking becomes more likely on

the target surface, impeding the laser's penetration. Consequently, the ablative effect of the laser diminishes. Notably, Cs element and nano-silica particles are thoroughly mixed in the solution, making the influence of nano-silica particles stacking weaker on them than on the target. Accordingly, as the concentration of nano-silica particles rises, the intensity of the Cs element characteristic spectral line begins to increase during normalization.

On the other hand, the enhancement effect of nano particles on LIBS signals is also affected by factors such as the size and uniformity of nano particles distribution [30]. As illustrated in Fig. 2(d), with an increase in nano particle size, the intensity values of Cs element analysis spectral lines exhibit a trend of initially increasing, then decreasing, and finally gradually increasing. This phenomenon is attributed to the existence of an optimal value for the ratio of nano particle diameter to particle spacing, i.e., the optimal nano particle stacking density. When the concentration of nano particles remains constant, an increase in nano particle size results in a higher ratio of size to spacing. At a nano-silica particles size of 50 nm, the optimal stacking density is achieved. However, surpassing this optimal value leads to increased aggregation, reducing field enhancement and resulting in a decrease in the enhancement effect on the intensity values of the analysis spectral lines [31]. With further increasing the particle size, CPLA exhibits a more optimal focusing effect on the laser, leading to a slight rise in the intensity values of the analysis spectral lines. Moreover, during the drying process, as the nano particle size increases, the capillary force also increases, intensifying the aggregation effect [28]. Consequently, the enhancement effect on Cs element characteristic spectral lines is superior with low particle size compared to high particle size.

As depicted in Fig. 3(a) and Fig. 3(c), during LIBS experiments, laser focusing ablates the surface of the target material, generate plasma. Owing to the Gaussian distribution of the laser energy, the target surface exhibits an ablative area with uneven depth between the middle and edge. In contrast, the addition of nano-silica particles to the target surface can replicate the function of CPLA and improve the surface roughness. Consequently, this results in a more uniform depth of the ablation area on the target surface.

Utilizing a white light interferometer for 3D scanning of the surface morphology of laser-ablated target materials during LIBS and NELIBS conditions reveals the outcomes depicted in Fig. 3(b) and Fig. 3(d). Notably, when nano-silica particles are present, there is a discernible uniformity in the depth of the ablation area on the target surface. This observation supports the hypothesis that the incorporation of a specific quantity of nano-silica particles onto the target surface can augment the laser ablation efficacy.

In conclusion, nano-silica particles with a particle size of 50 nm and a concentration of 0.1 mg/mL have demonstrated the most significant enhancement effect on the LIBS spectral signal. To investigate the influence of these nano-silica particles on the sensitivity of Cs element detection in LIBS, added Cs solutions of varying concentrations to the nano-silica particles of the specified size and concentration. Following ultrasonic mixing for 5 min, 200 µL of each solution was dripped onto the target surface for natural drying. Figure 4 illustrates the variation of LIBS analysis line intensity values with Cs element reference concentration, with and without nano-silica particles. At low concentrations, a discernible linear relationship exists between Cs element reference concentration and analysis line intensity values. However, it becomes apparent that in NELIBS, the linear fit between Cs element concentration and analysis line intensity values is stronger, with the analysis line intensity values showing a slight increased under the same element concentration.

By utilizing 207 data points within the wavelength range of 800.02 nm to 810.04 nm, where no apparent characteristic peaks are observed, as background spectra, the limit of detection (LOD) under different experimental conditions can be determined. This is achieved by calculating the ratio of three times the standard deviation of the background

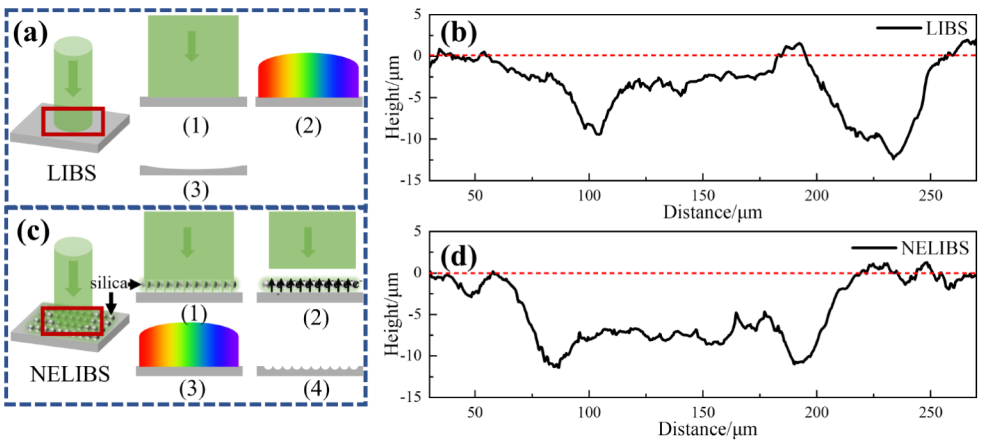

Fig. 3 Effect of nano-silica particles on laser ablation target. (**a**) Schematic Diagram of Laser Ablation in LIBS; (**b**) Cross-sectional Diagram of Laser Ablation Region in LIBS; (**c**) Schematic Diagram of Laser Ablation in NELIBS; (**d**) Cross-sectional Diagram of Laser Ablation Region in NELIBS

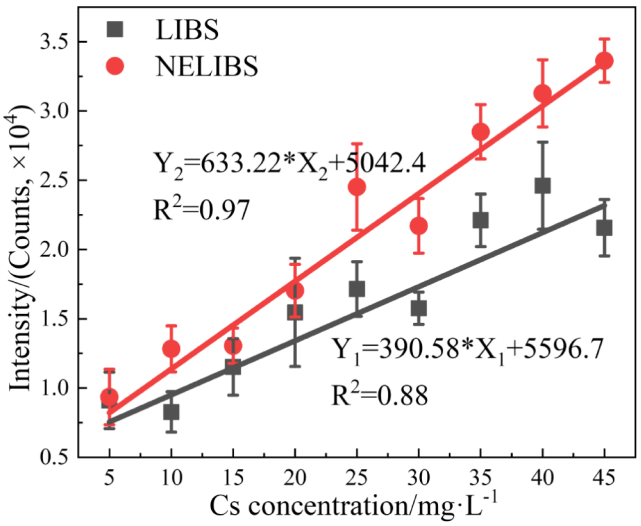

Fig. 4 Influence of nano-silica particles on the sensitivity of LIBS Detecting Cs element

spectra to the corresponding calibration curve slope. The LOD for LIBS and NELIBS are found to be 0.74 mg/L and 0.45 mg/L, respectively. Notably, at a Cs element concentration of 5 mg/L, both LIBS and NELIBS exhibit significantly pronounced characteristic peak signals. According to the limit of quantitation (LOQ) formula, $LOQ = 10\sigma_{blank}/S$, the LOQ under LIBS and NELIBS conditions are determined to be 2.45 mg/L and 1.51 mg/L, respectively.

Furthermore, the comparative analysis of the complete LIBS spectra under the three distinct conditions, as depicted in Fig. 5, reveals varying degrees of enhancement in the LIBS characteristic spectra of Mg, Cu, Ca, Fe, and Na within the target. With the exception of the Fe I 370.79 nm, Fe I 370.92 nm, Fe I 372.26 nm, Fe I 372.76 nm, Fe I 373.33 nm, Fe I 374.34 nm, and Fe I 377.83 nm characteristic spectral lines, which require the presence of nano-silica particles for excitation, hindering the calculation of the enhancement factor (E.F.) via the ratio of characteristic spectral line peaks between NELIBS and LIBS. Subsequently, the E.F. for the

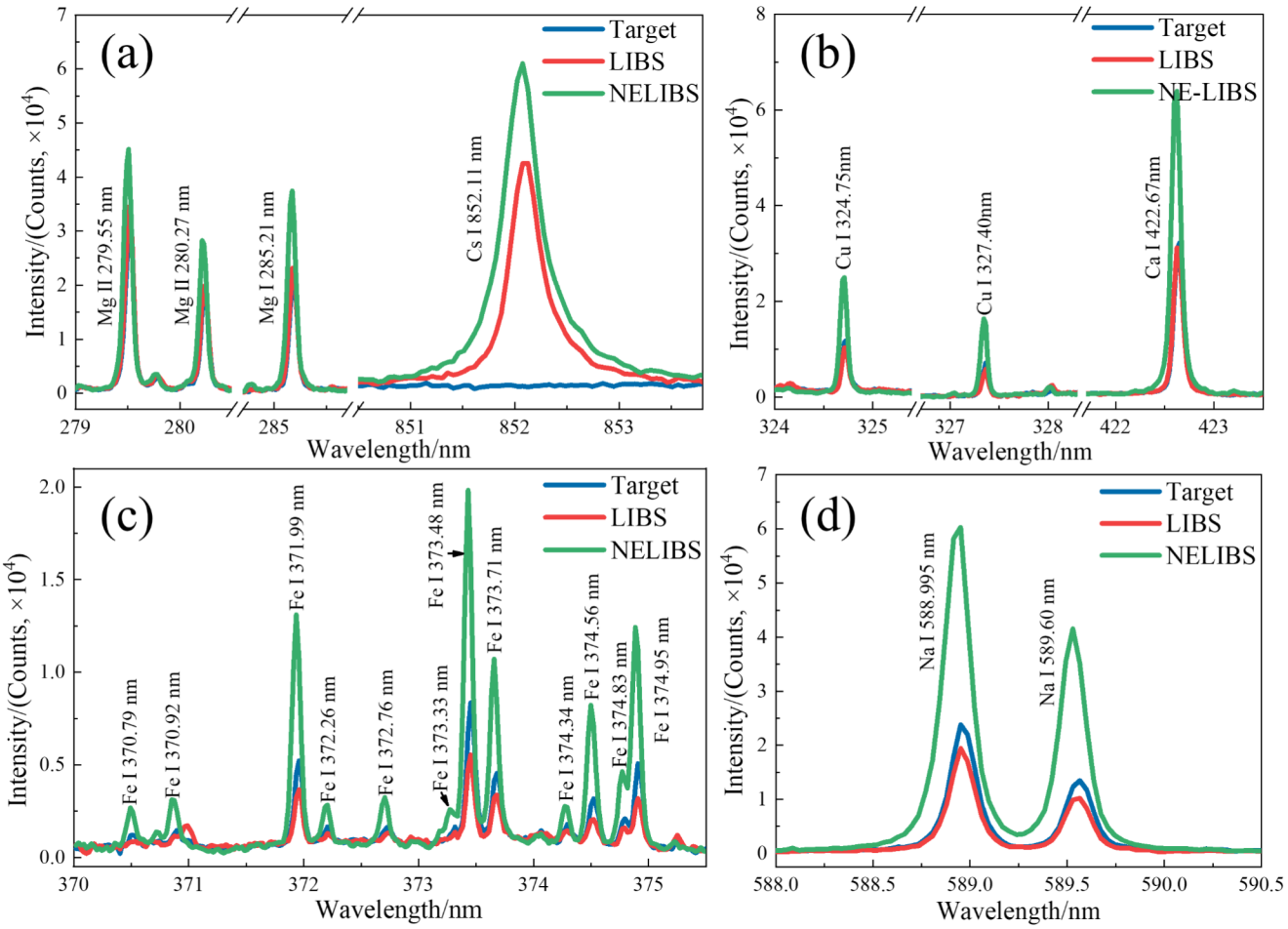

Fig. 5 Effect of nano-silica particles on LIBS spectra of different element in the target. "Target": dripping only alcohol on the target surface; "LIBS": dripping only cesium acetate solution on the target surface: "NELIBS": simultaneously dripping cesium acetate solution and nano-silica particles on the surface. (**a**) Mg and Cs; (**b**) Cu; (**c**) Fe; (**d**) Na

Table 1 The peaks information of the plasma spectra on LIBS and NELIBS in the target's element

Sp.	λ/nm	gA/S^{-1}	E_{up}/eV	E.F.	Sp.	λ/nm	gA/S^{-1}	E_{up}/eV	E.F.
Mg II	279.55	1.04×10^{9}	4.43	1.31	Fe I	373.71	1.27×10^{8}	3.37	3.34
Mg II	280.27	5.14×10^{8}	4.42	1.64	Fe I	374.56	8.05×10^{7}	3.40	4.13
Mg I	285.21	1.47×10^{9}	4.35	1.62	Fe I	374.95	6.87×10^{8}	4.22	4.68
Cu I	324.75	5.58×10^{8}	3.82	2.42	Ca I	422.67	2.18×10^{8}	2.93	2.07
Cu I	327.40	2.75×10^{8}	3.79	3.41	Na I	588.995	2.46×10^{8}	2.10	3.10
Fe I	371.99	1.78×10^{8}	3.33	4.04	Na I	589.60	1.23×10^{8}	2.10	4.20
Fe I	373.49	9.91×10^{8}	4.18	4.12					

Note "Sp." and "E.F." correspond to "Species" and "Enhancement Factor", respectively

remaining characteristic spectra is calculated and summarized in Table 1.

It has been clearly observed from the data listed in Table 1 that the deposition of nano-silica particles on the surface of the target has had a certain enhancement effect on the spectral intensity of the elements in the target. This enhancement has not been limited to specific elements or characteristic spectral lines. Therefore, enhancing the LIBS characteristic spectral signal by using nano-silica particles has proven to be a feasible method.

4 Conclusions

This article validates the capability of nano-silica particles to enhance the detection sensitivity of LIBS technology for Cs element. It investigates the influence of nano-silica particles with various concentrations and sizes on the intensity of analytical spectral lines. Utilizing a white light interferometer, it obtains the 3D morphology of the ablation area on the target surface. Under optimal parameters of nano-silica particles, a calibration curve is established for LIBS detection of Cs element. The research results indicate that in NELIBS experiments, the speed of target movement significantly affects the signal quality of the sample being tested. Additionally, incorporating suitable parameters of nano-silica particles into LIBS can achieve a certain enhancement effect on the characteristic spectral line intensity of measured elements. When nano-silica particles are evenly spread on the target surface, optimal laser ablation quality is attained, leading to an E.F. of LIBS characteristic spectral signals of elements in the target material by 1.3 to 4.7 times. Ultimately, the LOD of LIBS for Cs element is reduced from 0.74 mg/L to 0.45 mg/L, and the LOQ is decreased from 2.45 mg/L to 1.51 mg/L. In addition, the nano-silica particles have also had a certain enhancement effect on the spectral signal of elemental properties in the target, contributing positively to the application of NELIBS technology in on-site detection of trace nuclides.

Acknowledgements This work was supported by the National Natural Science Foundation of China (12374266, 12105131, 12027809), the National Key Research and Development Program of China (No. 2022YFE0103900) and the Fundamental Research Funds for the Central Universities (lzujbky-2022-ey05, lzujbky-2023-stlt01).

Author contributions The authors confirm contribution to the paper as follows. Study conception and design were done by S. W. and Z. L. S. W. performed the experiment and did analysis and interpretation of the results. Z. W. , S. S. , J. Y. , and B.H reviewed the results, S. S. , B. H. ,Z. L. provided lab facilities, and supervised the project. S.W. wrote the initial manuscript draft. C.Y. prepared Fig. 1. Z.L. refine the language expression of the article. J. Y. has conducted supplementary experiments during the revision of this manuscript. All authors have read and agreed to the published version of the manuscript.

Data availability No datasets were generated or analysed during the current study.

Declarations

Competing interests The authors declare no competing interests.

References

1. D. Salahel, F. Mahmoud, Oral and dermal exposure to natural radionuclides and heavy metals in water and sediments of Nile River, Qena, southern Egypt[J]. Sci. Rep. **13**(1), 22098 (2023). https://doi.org/10.1038/s41598-023-49389-3
2. H. Feng, Y. Wang, N. Li et al., Effects of biochar pyrolysis temperature on uranium immobilization in soil remediation: revealed by 16S rDNA and metabolomic analyses[J]. J. Hazard. Mater. **466**, 133502 (2024). https://doi.org/10.1016/j.jhazmat.2024.133502
3. Y. Fakhri, T. Mahmudiono, V. Ranaei et al., The concentration of Radionuclides (Lead-210, Polonium-210, and Cesium-137) in the muscle of Sardine Fish: a Global Systematic Review, Meta-analysis, and exposure Assessment [J]. Biol. Trace Elem. Res. **201**(4), 2011–2021 (2023). https://doi.org/10.1007/s12011-022-03289-1
4. J. Lin, Z. Hao, J. Yang et al., The semi-quantitative analysis of hole defects in metal additive manufacturing components using LIBS[J]. J. Anal. At. Spectrom. **39**(2), 536–544 (2024). https://doi.org/10.1039/D3JA00320E
5. Y. Rao, L. Zeng, M. Wu et al., Transfer learning based on dynamic time warping algorithms to improve qualitative analysis and quantitative prediction of rocks over multiple LIBS instruments[J]. J. Anal. At. Spectrom. **38**(3), 693–703 (2023). https://doi.org/10.1039/D2JA00370H
6. L. Huang, Y. Chen, J. Wang et al., Online identification and classification of Gannan navel oranges with Cu contamination by LIBS with IGA-optimized SVM[J]. Anal. Methods. **15**(6), 738–745 (2023). https://doi.org/10.1039/D2AY01874H

7. E. Wan, Q. Zhang, L. Li et al., The online in situ detection of indoor air pollution via laser induced breakdown spectroscopy and single particle aerosol mass spectrometer technology[J]. Opt. Lasers Eng. **174**, 107974 (2024). https://doi.org/10.1016/j.optlaseng.2023.107974
8. X. Li, J. Huang, R. Chen et al., Chromium in soil detection using adaptive weighted normalization and linear weighted network framework for LIBS matrix effect reduction[J]. J. Hazard. Mater. **448**, 130885 (2023). https://doi.org/10.1016/j.jhazmat.2023.130885
9. C. Fabre, N.E. Ourti, C. Ballouard et al., Handheld LIBS analysis for in situ quantification of Li and detection of the trace elements (be, Rb and Cs)[J]. J. Geochem. Explor. 236106979 (2022). https://doi.org/10.1016/j.gexplo.2022.106979
10. Y. Zhang, T. Zhang, H. Li, Application of laser-induced breakdown spectroscopy (LIBS) in environmental monitoring[J]. Spectrochimica Acta Part. B: at. Spectrosc. 181106218 (2021). https://doi.org/10.1016/j.sab.2021.106218
11. Y. Xing, Q. Li, X. Ye et al., Quantitative analysis of hydrogen isotopes in hydrogen storage material using laser-induced breakdown spectroscopy[J]. Nuclear Mater. Energy. **31**, 101204 (2022). https://doi.org/10.1016/j.nme.2022.101204
12. S. Mittelmann, K. Touchet, X. Mao et al., Hydrogen isotope analysis in W-tiles using fs-LIBS[J]. Sci. Rep. **13**(1), 2285 (2023). https://doi.org/10.1038/s41598-023-29138-2
13. T. Delgado, L. García-Gómez, L.M. Cabalín et al., Investigation on the origin of molecular emissions in laser-induced breakdown spectroscopy under Mars-like atmospheric conditions of isotope-labeled compounds of interest in astrobiology[J]. Spectrochimica Acta Part. B: at. Spectrosc. 179106114 (2021). https://doi.org/10.1016/j.sab.2021.106114
14. H. Andrews, C. Derrick Quarles, V. Bradley et al., Advancing elemental and isotopic analysis of Uranium Mineral inclusions: Rapid Screening via Laser-Induced Breakdown Spectroscopy and High-Resolution laser Ablation-ICP-MS Mapping[J]. Microchem. J. **196**, 109605 (2024). https://doi.org/10.1016/j.microc.2023.109605
15. M. Gaft, L. Nagli, A. Gorychev et al., High-resolution LIBS and LIBS-MLIF of REE molecular emission in laser-induced plasma[J]. Spectrochimica Acta Part. B: at. Spectrosc. **204**, 106667 (2023). https://doi.org/10.1016/j.sab.2023.106667
16. A. Metzinger, É. Kovács-Széles, I. Almási et al., An Assessment of the potential of Laser-Induced Breakdown Spectroscopy (LIBS) for the analysis of Cesium in Liquid samples of Biological Origin[J]. Appl. Spectrosc. **68**(7), 789–793 (2014). https://doi.org/10.1366/13-07297
17. M. Ramli, A. Khumaeni, K.H. Kurniawan et al., Spectrochemical analysis of Cs in water and soil using low pressure laser induced breakdown spectroscopy[J]. Spectrochimica Acta Part. B: at. Spectrosc. **132**, 8–12 (2017). https://doi.org/10.1016/j.sab.2017.03.017
18. N. Li, E. Harefa, W. Zhou, Nanosecond laser preheating effect on ablation morphology and plasma emission in collinear dual-pulse laser-induced breakdown spectroscopy[J]. Plasma Sci. Technol. **24**(11), 115507 (2022). https://doi.org/10.1088/2058-6272/ac8039
19. X. Jin, T. Gu, Y. Zhan et al., A review: experimental and applied research of double-pulse laser-induced breakdown spectroscopy[J]. Appl. Spectrosc. Rev. 1–44 (2024). https://doi.org/10.1080/05704928.2024.2320146
20. M. Huang, S. Wu, Z. Liu et al., Quantitative analysis of Cu in pig feed by microwave-assisted laser-induced breakdown spectroscopy[J]. Appl. Phys. B **129**(11), 167 (2023). https://doi.org/10.1007/s00340-023-08110-y
21. Y. Wang, Y. Jia, L. Gao et al., The effects of cavity diameter and material type of spatial confinement on intensity of laser-induced breakdown spectroscopy[J]. Phys. Scr. **98**(1), 015610 (2023). https://doi.org/10.1088/1402-4896/aca8d9
22. V. Kiris, J. Savovic, A. Nevar et al., Laser-induced breakdown spectroscopy analysis of water solutions deposited on PTFE surface: influence of copper oxide nanoparticles and NELIBS effect[J]. Spectrochimica Acta Part. B: at. Spectrosc. 187 (2022). https://doi.org/10.1016/j.sab.2021.106333
23. J.B. Jedlicki, D. Tellbach, B. Subirana, Metal Particle Detection Methods and their use for freeze-dried vaccine inspection: a Review[J]. IEEE Sens. J. 640–62 (2023). https://doi.org/10.1109/JSEN.2023.3324278
24. M. Wang, L. Jiang, S. Wang et al., Multiscale Visualization of Colloidal Particle Lens Array Mediated Plasma Dynamics for Dielectric Nanoparticle enhanced Femtosecond Laser-Induced Breakdown Spectroscopy[J]. Anal. Chem. **91**(15), 9952–9961 (2019). https://doi.org/10.1021/acs.analchem.9b01686
25. Z. Salajková, M. Holá, D. Prochazka et al., Influence of sample surface topography on laser ablation process[J]. Talanta. **222**(15), 121512 (2021). https://doi.org/10.1016/j.talanta.2020.121512
26. L.M. Cabalín, D. Romero, J.M. Baena et al., Effect of surface topography in the characterization of stainless steel using laser-induced breakdown spectrometry[J]. Surf. Interface Anal. **27**(9), 805–810 (1999)
27. I. Lopez-Quintas, V. Piñon, M.P. Mateo et al., Effect of surface topography in the generation of chemical maps by laser-induced plasma spectroscopy[J]. Appl. Surf. Sci. **258**(23), 9432–9436 (2012). https://doi.org/10.1016/j.apsusc.2012.04.026
28. M. Khan, S. Haq, Q. Abbas et al., Improvement in signal sensitivity and repeatability using copper nanoparticle-enhanced laser-induced breakdown spectroscopy[J]. Spectrochimica Acta Part. B: at. Spectrosc. **195**, 106507 (2022). https://doi.org/10.1016/j.sab.2022.106507
29. F. Zhang, Q. Wang, Y. Jiang et al., Effect of gold nanoparticle concentration on spectral emission of AlO molecular bands in nanoparticle-enhanced laser-induced Al plasmas[J]. J. Anal. At. Spectrom. **38**(2), 422–428 (2023). https://doi.org/10.1039/D2JA00379A
30. N. Chen, X. Shen, C. Wang et al., Elemental analysis of liquid samples by nanoparticle-enhanced laser-induced breakdown spectroscopy: using ordered nano-arrays with a tunable nanoparticle size and inter-particle distance[J]. J. Anal. At. Spectrom. **39**(2), 401–407 (2024). https://doi.org/10.1039/D3JA00327B
31. M. Dell'aglio, R. Alrifai, De A. Giacomo, Nanoparticle enhanced laser Induced Breakdown Spectroscopy (NELIBS), a first review[J]. Spectrochimica Acta Part. B: at. Spectrosc. **148**, 105–112 (2018). https://doi.org/10.1002/9781119758396.ch8